Journal of Systems Engineering and Electronics
Vol. 32, No. 4, August 2021, pp.731 – 747

Investigations and prospects of Fabry-Perot antennas: a review

LIU Zhiming[1,2], BORNEMANN Jens[1,*], LIU Shaobin[2], and KONG Xiangkun[2]

1. Department of Electrical and Computer Engineering, University of Victoria, Victoria V8W 2Y2, Canada;
2. College of Electronic and Information Engineering, Nanjing University of Aeronautics and Astronautics, Nanjing 210016, China

Abstract: Fabry-Perot (FP) antennas have characteristics of planar structures combined with high gain, and they have been widely used in wireless communications. With the progress of ongoing research, FP antennas have achieved various capabilities, but many of them are still under development, such as low-profile, wideband, circular polarization, multi-band, low-radar cross section (RCS) and reconfigurable features. This paper discusses the theoretical analysis methods and research progress of FP antennas, and explains the realization methods of different features of FP antennas. In order to indicate different technologies for realizing various capabilities, the key technologies and features of some of the latest designs are described. Finally, the research situation and prospects of FP antennas are summarized to guide their research directions in the future.

Keywords: Fabry-Perot (FP) antenna, partially reflective surface, research situation, research direction.

DOI: 10.23919/JSEE.2021.000063

1. Introduction

Fabry-Perot (FP) resonators are widely used in the fields of spectrum analyzers, lasers, filters and interferometers [1−5]. The FP resonator was first introduced into antenna design by Trentini in 1956 [6]. Subsequently, the antennas based on FP resonators have attracted increased attention due to their characteristics of simple configurations and high directivity. FP antennas are also known as FP cavity antennas, FP resonator antennas, electromagnetic band-gap (EBG) resonator antennas, 2-D leaky wave antennas, partially reflective surface (PRS) antennas and resonant cavity antennas [7−13]. FP antennas are mainly composed of a source antenna and a PRS. Compared with commonly used high-gain antennas, such as horns, lenses, arrays, reflectarrays/transmitarrays, FP antennas combine characteristics of simple design and easy fabrication.

In early days, although the FP antennas had various superior physical characteristics, they had not been developed vigorously in terms of performance due to their narrow operating bandwidths. With the continuous exploration of FP antennas, metasurfaces are added due to their electromagnetic wave control ability, which introduces more possibilities for performance improvement. FP antennas have made important breakthroughs with respect to certain properties, including high gain [14], low profile [15], wideband [16] and multi-band [17] operation, circular polarization [18], low-radar cross section (RCS) [19], and reconfigurability [20−23]. Currently, research related to FP antennas is still geared towards performance improvement.

Recently, metasurfaces have been widely used due to the fact that loading with suitable metasurfaces as PRSs can effectively improve the properties of FP antennas, such as increasing gain, expanding bandwidth, reducing mutual coupling, and reducing RCS [14−23]. Metasurfaces have the characteristics of diversified performance, easy assembly, planar structure, simple configuration and mature processing technology. These characteristics have greatly accelerated the applications of metasurfaces in FP antennas [7−23]. Metasurface units can be etched on the substrate of the source antenna or used to form PRSs. Source antennas can be a slot antenna [9], a microstrip antenna [15], a dipole antenna [24], a waveguide horn antenna [25], etc. The properties of the source antenna directly affect the features of FP antennas. In order to obtain an FP antenna that meets various requirements, introducing metamaterials with appropriate features into the FP antenna is an important means to achieve desired capabilities.

In this paper, firstly, we focus on two commonly em-

Manuscript received December 31, 2020.
*Corresponding author.
This work was supported by the National Natural Science Foundation of China (61671238; 61471368), the Fundamental Research Funds for the Central Universities (NJ20160008; 56XAA19052), the Jiangsu Planned Projects for Postdoctoral Research Funds (1601009B), the Equipment Advanced Research Foundation of China (61402090103), and the Natural Sciences and Engineering Research Council (NSERC) of Canada.

ployed theoretical analysis methods of FP antennas, and discuss their advantages and disadvantages. Secondly, the research status and key technologies of various capabilities of FP antennas are summarized in detail. Finally, the research prospects of FP antennas are summarized, which can indicate research directions for FP antennas in the future.

2. Theoretical analysis method

A theoretical analysis method suitable for the FP cavity structure is the key to the precise design of an FP antenna with specified capabilities. There are some reports that have thoroughly discussed the analysis theory. These analysis methods mainly include ray tracing methods [6,26], leaky wave theory [27−30], and transmission line (TL) methods [31−34]. Ray tracing, leaky-wave theory, and TL method are the most commonly used analysis methods for designing FP antennas. The following will briefly explain their applications in FP antennas.

2.1 Leaky wave analysis

FP antennas can be analyzed by the leaky-wave theory, and the related model is shown in Fig. 1.

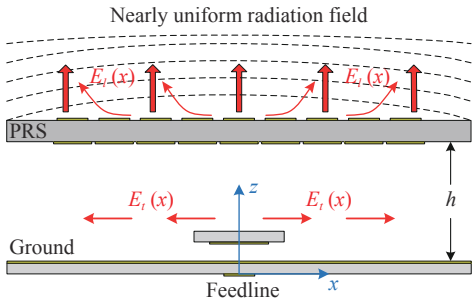

Fig. 1 Leaky-wave model of FP antennas

The ground of the source antenna and the PRS form an FP cavity. h represents the height of the cavity. When the source antenna is excited, the electromagnetic wave $E_t(x)$ radiated by the source antenna propagates from the center to the border in the cavity. The electromagnetic waves propagating in the cavity partly pass through the PRS and leak out of the cavity to generate leaky waves $E_l(x)$ due to the fact that the PRS has partial reflection characteristics. The amplitude and phase of the leaky-wave can be expressed [30] as

$$\varphi_l(x) = \theta_{\mathrm{PRS}}(x) - \mathrm{sgn}(x)\int_0^x \beta(\zeta)\mathrm{d}\zeta, \tag{1}$$

$$|E_l(x)| = C\sqrt{\alpha(x)}E_0\mathrm{e}^{-\mathrm{sgn}(x)\int_0^x \alpha(\zeta)\mathrm{d}\zeta}, \tag{2}$$

where θ_{PRS} represents the transmission phase of the PRS, ζ represents the position coordinates in the x direction, E_0 represents the source field, C represents a constant variable, $\mathrm{sgn}(x)$ is the signum function at position x inside the cavity, and α and β represent the attenuation and phase constants, respectively.

From (1) and (2), it can be seen that the amplitude of the leaky wave is related to the attenuation constant, and the phase of the leaky wave is related to the phase constant. Non-uniform amplitude distribution leads to a low aperture efficiency of FP antennas, while non-uniform phase distribution leads to energy divergence. According to the leaky wave model, improving the performance of the FP antenna is related to the design of a PRS with the desired attenuation and phase constants.

Leaky-wave analysis is more effective and accurate for different configurations of FP antennas compared with other methods. The transverse equivalent network model can be used to derive the formula of the beam angle, gain, beamwidth, leaky-wave phase and attenuation constants of the FP antenna [35]. The propagation constant depends on the reflection coefficient of the PRS and the height h of the FP cavity. Generally, the attenuation and the phase constants are strongly related to each other, and mutual interference occurs when the amplitude distribution and phase distribution of the leaky wave need to be independently modulated, which poses a greater challenge to improving the properties of FP antennas.

2.2 Ray tracing method

The ray tracing method is one of the most commonly used methods to analyze the performance of FP antennas [6,26]. Two reflecting surfaces are placed in parallel to construct the FP resonant cavity, and a source antenna is placed inside the cavity, as shown in Fig. 2.

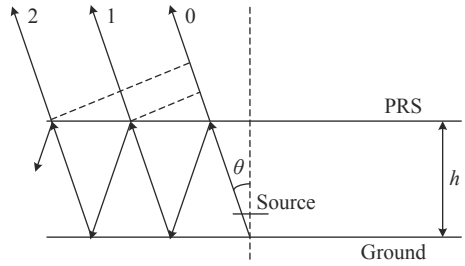

Fig. 2 Ray tracing model of FP antennas

As the source antenna is excited, the electromagnetic waves are repeatedly reflected and transmitted through the PRS, and the transmitted waves undergo in-phase superposition after FP resonance, thereby achieving the purpose of gain enhancement. In the ray tracing method, an FP cavity model with infinite reflectors is utilized to analyze the properties of FP antennas, so the source inside the cavity can be regarded as a point source. In order to excite the resonance of the FP cavity, the wave path dif-

ference between transmitted waves passing through PRS needs to be an integer multiple of 2π. Also, it is assumed that the electromagnetic waves radiated by the FP antenna propagate along the boresight direction, i.e., $\theta = 0°$. Therefore, the derived FP resonance condition and the maximum relative directivity D_r in the boresight direction are expressed as

$$\varphi_1 + \varphi_2 - \frac{4\pi}{\lambda}h = 2N\pi,\ N = 0, \pm1, \pm2, \cdots \tag{3}$$

$$D_r = 10\log\left(\frac{1+R}{1-R}\right) \tag{4}$$

where h is the cavity height ($h \neq 0$), R and φ_1 represent the reflection amplitude and the phase of the PRS respectively, and λ is the operating wavelength in free space. The metal ground has the reflection amplitude of $R_{GND} = 1$ and the reflection phase of $\varphi_2 = -\pi$ due to its total reflection characteristics.

Since approximate techniques and infinite reflectors have been used in the derivation of (3) and (4), the ray tracing method is not as accurate as the leaky-wave method for the theoretical analysis of FP antennas. The aperture size of the PRS has a significant influence on the antenna gain. Wang et al. [9] presented an equation of the aperture area for an FP antenna with a specified directivity, and its expression

$$A = \frac{10^{\frac{D}{10}}\lambda^2}{0.8\pi^2} \tag{5}$$

where D is the required directivity, $D = D_s + D_r$, and D_s is the directivity of the source antenna at the operating frequency.

The above elaborations provide the FP resonance condition of an FP antenna. It shows that the FP resonance is related to the reflection phases of the reflectors, the height of the cavity and the wavelength at the operating frequency. Also, the directivity of the FP antenna is related to the reflection amplitude of the PRS and the directivity of the source antenna at the operating frequency. The larger the reflection amplitude of the PRS, the greater the directivity of the FP antenna. Generally, $\varphi_1 \approx -\pi$, $\varphi_2 = -\pi$, the FP cavity has a height of $\lambda/2$ as $N = -2$. In order to excite the FP resonance, if N selects other integers, the cavity height will be increased and more energy will be dissipated, which will greatly affect the gain of the FP antenna.

2.3 TL method

The TL model can also be employed to analyze the radiation performance of FP antennas. Many studies on the properties of the resonant cavity structure have been conducted [31−34]. The geometric configurations of the FP antenna can be regarded as a cascade model of TL with different characteristic impedance. In [31], Jackson used the TL model to establish resonance conditions and simple asymptotic formulas for gain, bandwidth, and beamwidth. In the TL model, a shunt admittance is utilized to represent PRS, and the entire geometric configurations are equivalent by TLs with different properties and lumped elements. It can be found that the FP resonance conditions deduced by the TL model and the ray model are consistent. In [34], the normalized transmission coefficient was proposed to analyze and evaluate the directivity of FP antennas by employing the TL model. Therefore, the TL model provides convenience for designing FP antennas and also gives theoretical support for the performance analysis of FP antennas.

3. Performance realization

3.1 Low-profile

Generally, the cavity height of a traditional FP antenna is approximately one-half of the operating wavelength. With the development of high levels of integration in modern communication technology, new requirements are put forward for the profile height of FP antennas; some electronic devices are expected to use FP antennas with low profile for miniaturization. Many researchers have put forward relevant research reports in theory and technology to design FP antennas with low profile. These low-profile FP antennas can be divided into two categories: (i) dielectric-unfilled low-profile FP antennas; (ii) dielectric-filled low-profile FP antennas.

Dielectric-unfilled low-profile FP antennas are usually realized by modulating the reflection phase of reflectors. In 2005, Zhou et al. proposed a subwavelength metamaterial-based cavity to achieve a low-profile FP antenna, which reduced the height of the FP cavity to $\lambda/4$ [36]. In 2006, Wang et al. proposed a low-profile FP antenna by using a metamaterial ground plane (MGP) with the negative reflection phase as a reflector [37]. The cavity of the FP antenna was composed of a PRS formed by a metasurface and a periodic EBG structure. This design achieved a high directivity, and the height of the cavity was less than $\lambda/6$. In 2008, Kelly et al. proposed a low-profile FP antenna by adopting an artificial periodic ground with a specific reflection phase response [11]. The leaky-wave analysis has been employed to determine the complex propagation constant of the leaky-wave modes and the reduction effect of the profile of an FP antenna. This design realizes that the profile height varies from $\lambda/19.8$ to $\lambda/2$. In 2010, Costa et al. proposed a subwavelength tunable

low-profile FP antenna by using an active high-impedance surface (HIS) and a frequency selective surface (FSS) [38]. The active high-impedance surface was loaded with varactor diodes to achieve the tunable properties of the FP antenna. This design cannot only adjust the operating frequency, but also realize beam steering at the corresponding frequency. Also, it can realize a low-profile FP antenna at different operating frequencies; the cavity height at the minimum operating frequency was about $\lambda/13$.

Subsequently, dielectric-filled low-profile FP antennas were developed. In 2011, Zhu et al. presented a dielectric-filled low-profile FP antenna [39]. The FP antenna consisted of a PRS formed by a finite-size periodic metal patch array. The cavity was filled with a dielectric substrate, and the height of the cavity was only $\lambda/3.3$. It shows that by using a dielectric-filled cavity, the FP antenna can effectively achieve low profile combined with high gain and high radiation efficiency. In [40], Sun et al. proposed a dielectric-filled high-gain, low-profile FP antenna by using an artificial magnetic conductor (AMC), as shown in Fig. 3. By adjusting the parameters of the AMC structure, the appropriate reflection phase of the PRS is obtained so that the FP resonance response with an overall height of $\lambda/9$ is effectively excited. In 2013, Ji et al. presented a dielectric-filled FP antenna fed by a slot-coupled patch array [41]. It shows that the dielectric-filled FP antenna with the 2×2 slot-coupled patch array has a maximum gain of 15.5 dBi at 10.0 GHz. Compared with the traditional air-filled FP antenna, this antenna has a low profile, a high gain and a strong mechanical robustness. In 2014, Liu et al. introduced a substrate integrated waveguide (SIW) slot fed structure in a dielectric-filled low-profile FP antenna [42]. This antenna has a maximum gain of 13.5 dBi at 9.8 GHz and an overall height of $\lambda/8.3$, which achieves characteristics of a low profile, a high boresight gain and low backlobe levels. In 2015, Nguyen et al. developed a design of a planar low-profile high-gain dielectric-filled FP antenna [43]. This antenna was composed of an FSS and a planar feeding structure, which are both etched on a high-permittivity substrate. In 2018, Gao et al. proposed a 2×2 low-profile circularly polarized FP antenna array with a low-cost substrate-integrated waveguide feed network [44]. This design introduced an AMC structure on the ground, which reduced the height of the cavity to $\lambda/4$. Besides, an SIW feed network was used to generate electromagnetic waves with a phase difference of 90° at the four output ports so that the FP antenna radiated a circularly polarized wave.

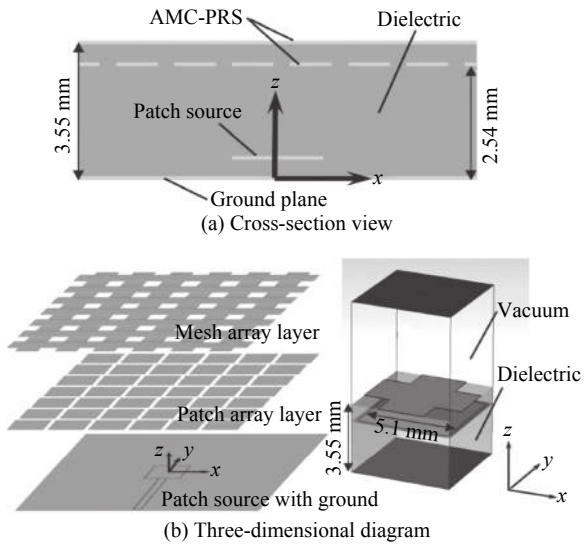

Fig. 3 Geometry of the low-profile FP antenna [40]

3.2 Wideband

In the early stage, FP antennas exhibit narrow-band characteristics, which severely restrict their range of applications. The bandwidth of FP antennas is mainly limited by the high Q-factor properties of FP cavities. The reflection coefficients of PRSs are important factors that directly affect the properties of FP antennas. The expansion of the impedance bandwidth of FP antennas can be realized by optimizing the reflection property of PRS and the FP resonant effect of the cavity, or by designing a source antenna with a wide operating band and a PRS with a positive reflection phase gradient band that matches the operating band. At present, there are two types of PRS to realize a wideband FP antenna. One is a printed PRS, and the other is an all-dielectric PRS.

The printed PRS is one of the important methods to realize a wideband FP antenna. In 2006, Ge et al. adopted an EBG structure, FSS structure and non-printed dielectric into a design of FP antennas, achieving wideband gain enhancement, a high aperture efficiency and low backlobe levels [45]. Meanwhile, Feresidis et al. proposed a high-gain wideband FP antenna by using a double-layer periodic metasurface [46]. This antenna was fed by a waveguide slot, and a double-layer periodic metasurface with positive reflection phase gradient characteristic was applied as PRS. This design can excite the FP resonance effect in a wide operating band. In 2008, Liu et al. presented a wideband FP antenna by using a gradient metasurface as the PRS [47]. It shows that loading the antenna with a suitable gradient metasurface can effectively expand the gain bandwidth. In 2010, Wu et al. realized a wideband FP antenna through a mushroom nail-

shaped gradient HIS structure [48]. As shown in Fig. 4, the antenna uses a periodic FSS structure as the PRS, and a mushroom nail-shaped gradient HIS structure is etched around the source antenna to correct the nonuniform phase and magnitude of the field distribution, thereby providing the FP antenna with a wider operating bandwidth and a higher aperture efficiency. In 2012, Ge et al. designed a wideband FP antenna by using a thin single-dielectric-slab PRS [49]. The PRS has a property of positive reflection phase gradient within the operating band of the source antenna, thereby exciting the FP resonance mode of the proposed antenna in a wide operating band. Also, Pirhadi et al. proposed a high-directivity wideband FP antenna fed by an aperture coupled microstrip patch antenna [50]. This design employs a parasitic patch to expand the operating band and uses a periodic FSS structure as the PRS to generate multiple separate resonance frequencies, thereby achieving an expansion of the antenna's operating bandwidth. In 2014, Konstantinidis et al. implemented a high-gain wideband FP antenna by using multilayer periodic metasurfaces as PRSs [8]. By designing appropriate reflection properties of the multilayer PRSs, the FP resonant mode was excited to achieve a high-gain and wideband FP antenna. Besides, Fig. 5 demonstrates a wideband FP antenna by employing an EBG consisting of two complementary FSS structures [9] which expand the operating bandwidth of the FP antenna due to their positive reflection phase gradient features. In this way, the FP resonant mode can be excited in a wide band.

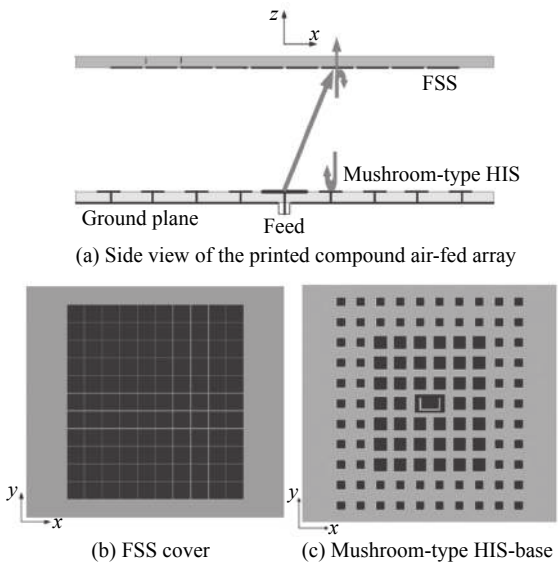

(a) Side view of the printed compound air-fed array

(b) FSS cover (c) Mushroom-type HIS-base

Fig. 4 Wideband FP antenna with a mushroom nail-shaped gradient HIS structure [48]

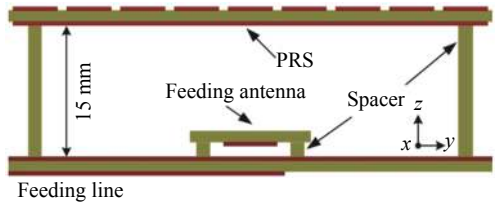

Fig. 5 Wideband FP antenna along with a PRS with positive reflection phase gradient [9]

Research on the bandwidth extension of FP antennas based on the printed PRS has made significant progress. However, due to the limitation of the reflection coefficients of the printed PRS, it is difficult to exceed the 3 dB gain bandwidth of FP antennas with printed PRS beyond 30% [8,9,45−50]. In order to seek a greater breakthrough in the bandwidth expansion of FP antennas, it was found that the use of non-printed dielectrics as PRSs can excite the FP resonant mode in a wider band, thereby achieving wideband FP antennas with a wide 3 dB gain bandwidth.

In 2005, a technique was proposed to increase the radiation bandwidth and gain of FP antennas, which relies on the number of sources and array spacing to optimize antenna performances [51]. In 2014, Hashmi et al. put forward a novel design of a wideband FP antenna by introducing a multilayer non-printed truncated dielectric PRS [52]. The multilayer dielectric PRS structure was truncated to expand the antenna bandwidth and improve aperture efficiency. In 2015, Hashmi et al. developed an FP antenna with an extremely small footprint by using a multilayer disc-type composite non-printed dielectric PRS [53]. In 2016, Hashmi et al. presented a single-layer dielectric PRS with a transverse permittivity gradient (TPG) to achieve an extremely wideband FP antenna with a large gain-bandwidth product (GBP) [13]. In [54], Baba et al. proposed a compact wideband FP antenna with a multilayer dielectric laminated TPG PRS, as shown in Fig.6. In 2018, Baba et al. proposed a simple compact wideband FP antenna by using a TPG PRS with a single high-permittivity dielectric substrate [55]. Also, Fig. 7 demonstrates a wideband FP antenna by employing a multilayer truncated thin dielectric PRS [56]. In Fig. 7, SMA means sub-miniature version A. PEC denotes the perfect electrical conductor. It can be seen from [13] and [53−56] that the use of a non-printed dielectric PRS can greatly expand the bandwidth of FP antennas compared with a printed PRS.

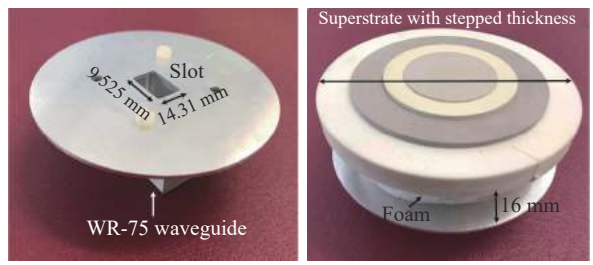

(a) Ground plane and slot-coupled WR-75 waveguide feed (b) Fabricated prototype

Fig. 6 Wideband FP antenna with a multiplayer dielectric laminated TPG PRS

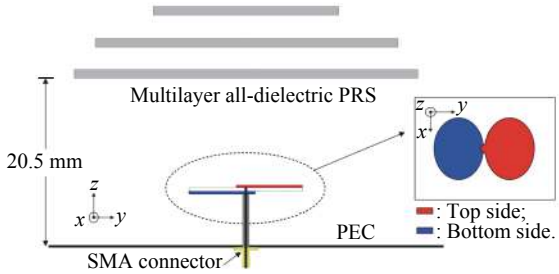

Fig. 7 Wideband FP antenna with multilayer all-dielectric PRS [56]

3.3 Multi-band

Antennas with multiple operating bands are required in some scenarios to achieve the multi-band communication capabilities of the equipment. Research on the multi-band FP antennas has attracted several researchers. In 2004, Lee et al. demonstrated a way to achieve high-gain dual-band FP antennas by controlling the defect mode of the EBG structure [17]. In 2007, Lee et al. proposed an ultra-thin FSS as a PRS to design a high-gain dual-band FP antenna. The dual-band and gain enhancement of the FP antenna was achieved by analyzing the FP resonance and quality factors of three printed PRSs [57]. In 2012, Zeb et al. combined a one-dimensional EBG structure and a stacked patch feed to construct a high-gain dual-band FP antenna [10]. They also presented a tri-band FP antenna with increased gain in three operating bands by designing a suitable reflection phase of the PRS which consisted of periodic printed dipoles [58].

FP antennas with multiple bandwidths are still under investigation. In 2017, Abdelghani et al. proposed a dual-band wideband FP antenna [59]. This antenna adopts a double-layer periodic PRS structure with dual-band response to obtain a wide 3 dB gain bandwidth in two operating bands. Also, Qin et al. developed a high-gain, low-profile tri-band FP antenna [60]. As shown in Fig. 8, this design adopts a two-layer FSS structure to obtain three FP resonant modes, of which two resonant modes are independently tuned by the two-layer FSS structure, and the third resonant mode is generated by the joint action of two FSS layers. In 2018, Chen et al. proposed a dual-band FP antenna with a shared-aperture FSS layer. The printed PRS can provide quasi-optimal reflection phases with high reflectivity in two frequency ranges [61].

Quite a few achievements have been made on FP antennas with multi-band and multi-polarization features. In 2016, Qin et al. proposed a shared-aperture dual-band dual-polarized high-gain FP antenna that can be potentially used in synthetic aperture radar [62]. The antenna works in both C-band and X-band by employing dual FSS layers to form two independent resonant cavities, thus making the choice of operating frequencies more flexible. Moreover, the antenna can accommodate the beam scanning capability by adjusting the phased array. In 2017, Xie et al. designed a reflective metasurface with different reflection phases for different polarized waves on the substrate of the feed antenna to achieve a high-gain, dual-polarized, dual-band FP antenna [63]. The source antenna was a dual-band patch antenna, which radiated different polarized waves in different bands. The FP resonances in two operating bands can be excited by adjusting the reflection phase of the metasurface. In 2018, Chen et al. demonstrated a dual-band, dual-orthogonal, circularly polarized (CP) FP antenna by adopting a chiral metamaterial (CMM) [64]. This FP antenna consists of a linearly polarized (LP) microstrip patch antenna and a CMM, as shown in Fig. 9. The CMM has the functions of converting an LP wave to a left-hand CP (LHCP) wave and an LP wave to a right-hand CP (RHCP) wave in two different bands, thereby realizing the FP antenna with different polarization characteristics within two operating bands.

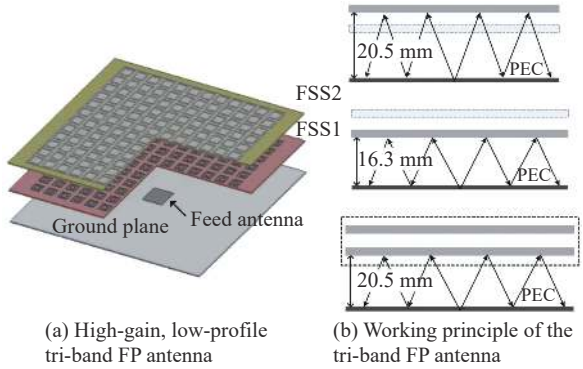

Fig. 8 Tri-band low-profile high-gain FP antenna [60]

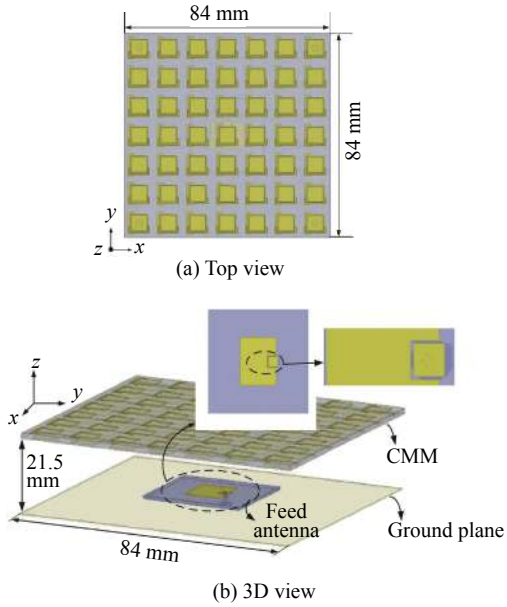

Fig. 9 Dual-band, dual-orthogonal, CP FP antenna with CMM [64]

3.4 Circular polarization

CP antennas are widely used in wireless communication

systems due to the fact that they can obtain a stable link between transmitting and receiving antennas when the signal polarization is not aligned, such as in satellite communications, radar systems, radio frequency identification (RFID), and electronic warfare [64−69]. The realization of CP FP antennas is mainly considered via the following two methods: (i) by employing a CP source antenna; (ii) by using an LP source antenna and a PRS with properties of converting LP to CP.

Using a CP source antenna is one of the important methods to realize a CP FP antenna. In 2006, Weily et al. used four LP stripline slot arrays to design a CP source antenna for an FP antenna [70]. The FP antenna has the advantages of high gain, simple configuration, low sidelobe levels, and stable axial ratio (AR) within the operating bandwidth. In 2015, Qin et al. proposed a wideband high-gain CP FP antenna by designing a CP microstrip patch antenna with quasi-L strips coupled feeding lines and a Wilkinson power divider [18]. In 2017, Liu et al. demonstrated a wideband high-gain CP FP antenna using a 2×2 CP microstrip patch antenna array [71]. In 2018, Tran et al. applied an Archimedean spiral antenna as the CP source antenna to design a wideband CP FP antenna [72]. Subsequently, in 2019, Cao et al. designed a CP FP antenna with wideband and high-gain characteristics using a CP magnetoelectric dipole antenna as a source [73]. Fig. 10 presents a low-profile high-gain CP FP antenna which adopts an ellipse-shaped dipole as a source [74]. This design uses an AMC to obtain a suitable reflection phase of the reflector, thereby reducing the height of the FP cavity and realizing a low-profile design of the FP antenna.

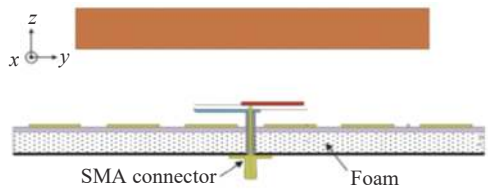

(a) Cross-section view

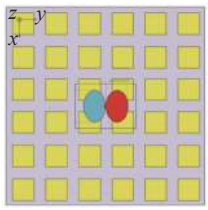

(b) Top view of the ridiator over AMC reflector

Fig. 10 Low-profile high-gain CP FP antenna [74]

The method of converting LP to CP waves is another important way to realize CP FP antennas. This method uses an LP antenna as the radiation source whose waves will be converted into CP waves through a PRS, thereby obtaining the CP FP antenna. In 2005, Diblanc et al. described a high directivity CP FP antenna by using an EBG structure [75]. This design uses a patch antenna as the radiator which can radiate an oblique 45° LP wave. The EBG grid structure converts the oblique 45° LP wave into a CP wave, thereby realizing a CP FP antenna. In 2014, Orr et al. designed a CP FP antenna using an anisotropic HIS and a double-sided PRS [76]. The radiated wave of the source antenna was an oblique 45° LP wave. The amplitude and phase of the reflection coefficient and the transmission coefficient of the PRS can be independently modulated by adjusting the parameters of the PRS unit. Moreover, combined with the features of HIS, the LP wave radiated by the source can be transformed into a CP wave after passing through a PRS. In 2017, Liu et al. presented a low-profile CP FP antenna consisting of a PRS, a non-standard AMC, and a 2×2 array that radiates LP waves along an oblique direction of 45° [77]. The use of the array design can expand the operating bandwidth of the CP FP antenna, improve the directivity and reduce sidelobe levels. In 2018, Ren et al. utilized a linear-to-circular polarization converter to achieve a high-gain low-RCS CP FP antenna [78]. This antenna adopts an LP patch antenna rotated by 45° on the horizontal plane as the radiator and an asymmetric metasurface as the polarization converter, as shown in Fig. 11. Also, an absorbing surface (AS) at the top of the asymmetric metasurface is employed to reduce the RCS of the antenna, while the PRS at the bottom forms an FP resonant cavity with an anisotropic HIS.

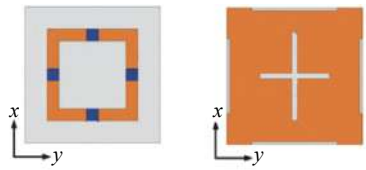

(a) Unit of the upper-layer metastructure

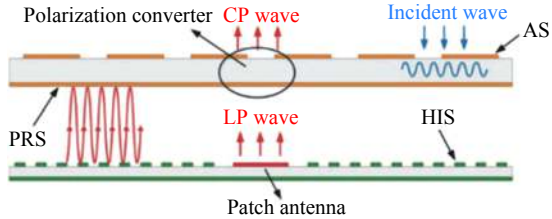

(b) Schematic model of the proposed antenna

Fig. 11 Low-RCS CP FP antenna with linear-to-circular polarization converter [78]

3.5 Reconfigurable features

With the development of highly integrated, intelligent, and multifunctional communication systems, antennas

with reconfigurable characteristics are more able to adapt to complex communication scenarios. The reconfigurable properties of FP antennas mainly include frequency reconfiguration, pattern reconfiguration, and polarization reconfiguration. It is mainly through the introduction of controllable elements to achieve the reconfigurable features of FP antennas, such as loading varactor diodes, personal identification number (PIN) diodes, and micro-electro-mechanical system (MEMS) switches.

3.5.1 Frequency reconfigurability

A frequency reconfigurable FP antenna mainly realizes the adjustable operating frequency under the premise of maintaining the radiation pattern and polarization characteristics, which can improve the anti-interference ability and enhance security for wireless communications. In 2008, Weily et al. presented a frequency reconfigurable FP antenna using an electrically controlled phase-agile reflection surface [79]. The array of phase-agile reflection cells with varactor diodes is etched on a thin substrate, and the operating frequency of the antenna can be tuned by adjusting the voltage applied to the varactors. In 2016, Huang et al. proposed a frequency reconfigurable FP antenna with low RCS characteristics by employing a two-layer metastructure [23]. The FP cavity was formed by a PRS and a tunable reflection phase surface to improve the antenna gain, and the frequency reconfigurable characteristics of the antenna were realized by controlling the voltage of the varactor diodes which loaded the tunable reflection phase cells. The AS on the top-layer metastructure was used to absorb the incident waves for wideband RCS reduction of the antenna. In 2017, Xie et al. combined a reconfigurable PRS with PIN diodes to design a frequency-reconfigurable FP antenna [80]. The PRS is shown in Fig. 12. The stub V connects the anode of the DC source, and the stub ground connects the cathode of the DC source. This antenna achieves reconfigurable frequency characteristics by controlling the working state of the PIN diodes within two operating bands.

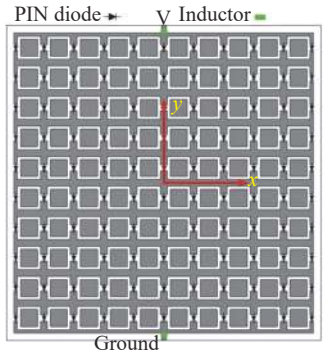

Fig. 12 Reconfigurable PRS with PIN diodes [80]

3.5.2 Radiation pattern reconfigurability

FP antennas with radiation pattern reconfigurability realize the reconfiguration characteristics under the premise of maintaining the operating frequency and polarization. Usually, there are three methods to achieve radiation pattern reconfigurable of FP antennas: (i) using a source antenna with radiation pattern reconfigurability; (ii) adjusting the state of the controllable unit on the reflectors; (iii) using a dynamically adjustable cavity.

The use of a source antenna with reconfigurable radiation pattern is one of the important methods to realize the radiation pattern reconfiguration of FP antennas. In 2004, Hao et al. used a uniplanar compact EBG structure to design the beam shaping of an FP antenna [81]. The beam shaping was achieved by shifting the defects from the center of uniplanar compact EBG cavities. In 2014, Debogovic et al. employed a phased array and a reconfigurable PRS to obtain an FP antenna with dynamic control of independent beam scanning and beamwidth [82]. The beamwidth was controlled by modulating the bias voltages of the varactors which were embedded in the PRS, while the beam scanning was regulated by a small phased array source antenna.

Adjusting the controllable element of the cavity reflectors is another important method to realize radiation pattern reconfigurable FP antennas. The FP antenna has two reflectors. One reflector is integrated on the source antenna, and the other reflector is used as a PRS. Therefore, controllable elements can be loaded on the two reflectors to realize radiation pattern reconfigurable FP antennas. In 2010, Debogovic et al. achieved dynamic control of the beamwidth of an FP antenna by employing a reconfigurable PRS [83]. The working state of the varactor diodes imbedded in the PRS was controlled by adjusting the voltages of the bias circuits so that the reflection phase of the PRS was modulated, thereby realizing the dynamic beamwidth control of the antenna. And then, in 2013, Debogovic et al. loaded the PRS with MEMS elements to achieve dynamic control of the beamwidth of the FP antenna [84]. The reflection coefficient of the PRS was tuned by adjusting the state of the MEMS elements, so as to obtain the beamwidth reconfigurability. Moreover, the PRS has characteristics of polarization insensitivity, which was employed for independent beamwidth control of dual linear polarizations. In 2016, Guzman-quiros et al. developed an FP antenna with an electronically controlled beam scannable in two dimensions [21]. This design employed a tunable HIS on the substrate of the source antenna, and divided the HIS into four controllable areas. The reflection coefficients of the four subareas are independently controlled by changing the

voltages of the varactor diodes in each area, and the combined control of the four sub-areas can greatly improve the capability of beam scanning. In 2019, Ji et al. used a reconfigurable PRS to obtain an FP antenna with two-dimensional beam-steering features [85]. This antenna consists of a probe-fed square patch antenna and a PRS loaded with PIN diodes, as shown in Fig. 13. The reconfigurable PRS is divided into four sections. Through independent or combined control of the status of the PIN diodes inserted in each section, the FP antenna produces ten different radiation modes. V1, V2, V3 and V4 are four different DC voltages.

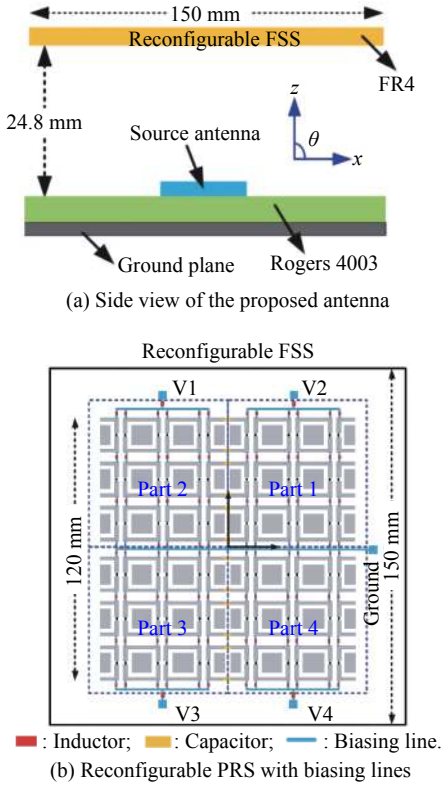

Fig. 13 FP antenna with two-dimensional beam-steering [85]

Recently, a novel method was proposed to realize reconfigurable radiation patterns of FP antennas by modulating the cavity operating modes. In 2016, Sultan et al. incorporated a magnetized ferrite dielectric in the FP cavity to achieve a reconfigurable radiation pattern of the FP antenna [86]. This method uses phased array technology to excite the FP resonance mode, and applies controllable phase delays to the two feed ports. The introduction of the magnetized ferrite medium in the cavity expands the beam scanning angle of the FP antenna and reduces the sidelobe levels. In 2019, Lan et al. adopted a movable FP cavity to achieve beam scanning of an FP antenna [87]. The antenna consists of a slot-fed patch antenna and a superstrate consisting of multilayer perforated dielectrics with different dielectric constants, as shown in Fig. 14. The beam of the antenna is controlled by moving the multi-layer dielectric structure above the source antenna. The greater the offset between the source antenna and the superstrate, the larger the scan angle of the beam.

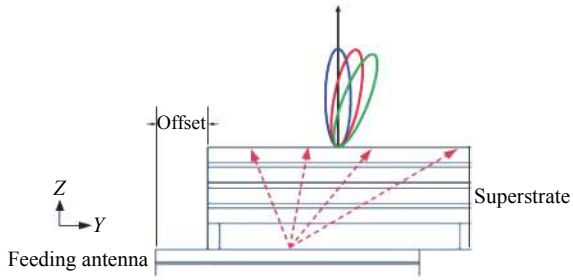

Fig. 14 Beam scanning FP antenna by moving the superstrate [87]

3.5.3 Polarization reconfigurability

Polarization reconfigurable antennas have characteristics of enhancing channel capacity [88], suppressed multipath effects [89] and frequency reusability [90], which has important applications for improving the quality and security of communications. Polarization reconfigurable antennas should achieve reconfigurable polarization characteristics under the premise of maintaining the operating frequencies and radiation patterns. According to the polarization classification, the polarization reconfigurable switching modes of antennas are divided into three categories: switching between horizontal polarization (HP) and vertical polarization (VP), switching between RHCP and LHCP, and switching between LP and CP. Performance of polarization reconfigurable FP antennas has improved, but there remain some issues that need to be addressed. Usually, there are two methods to realize the polarization reconfiguration properties of FP antennas: (i) using a polarized reconfigurable antenna as the source antenna; (ii) using a polarized reconfigurable metasurface as the PRS.

Using a polarization reconfigurable antenna as the source is one of the common methods to achieve polarization reconfigurability in an FP antenna. In 2013, Han et al. designed a polarization reconfigurable FP antenna using a CP reconfigurable source antenna [91]. This antenna was embedded with a polarization switchable source antenna in the cavity, which can produce polarization switching between RHCP and LHCP by controlling the switchable slots. In 2014, Vaidya et al. combined a CP reconfigurable source antenna with shorting posts to achieve an RHCP and LHCP reconfigurable FP antenna [92]. In 2018, Lian et al. proposed a broadband polarization reconfigurable FP antenna with polarization recon-

figurable patch element and patch array that can be switched between HP and VP by controlling the on/off state of the four pairs of PIN diodes [20]. In 2020, Tran et al. incorporated two PIN diodes (D_1, D_2) into a reconfigurable microstrip patch to design a polarization reconfigurable FP antenna, as depicted in Fig. 15, which can switch the polarization mode between dual-sense CP and single LP [93]. V_1 and V_2 represent two different DC voltages.

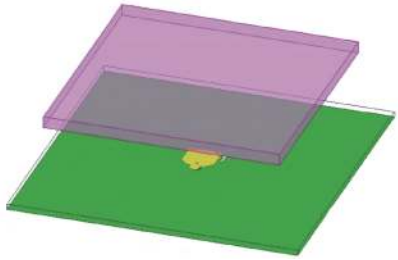

(a) 3-D view of the antenna

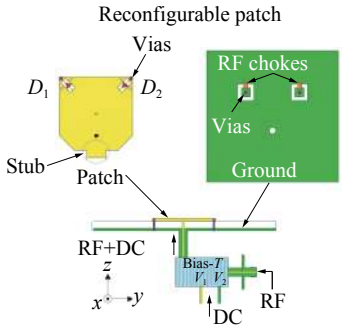

(b) Detailed configuration of the reconfigurable patch

Fig. 15 Polarization reconfigurable FP antenna with reconfigurable patch [93]

Employing a metasurface with polarization reconfigurable capability as PRS is another way to realize polarization reconfigurable FP antennas. In 2017, Li et al. proposed an RHCP and LHCP reconfigurable FP antenna using an electronically reconfigurable polarizer [94]. By changing the working state of the PIN diodes on the top and bottom of the polarizer, the LP wave radiated by the source antenna was converted into an RHCP or LHCP. In 2020, Ni et al. combined a planar metasurface and a slot antenna to design a polarization reconfigurable FP antenna [95] where the metasurface acts as the PRS. When the relative positions between the PRS and the slot antenna are changed by rotation, the polarization of the antenna can be reconfigured into LP, RHCP and LHCP. Later, as depicted in Fig. 16, Zhang et al. also utilized the method of manually rotating the PRS to obtain a polarization reconfigurable FP antenna whose polarization mode can be switched between LP, RHCP and LHCP through a polarization conversion metasurface (PCM) [96].

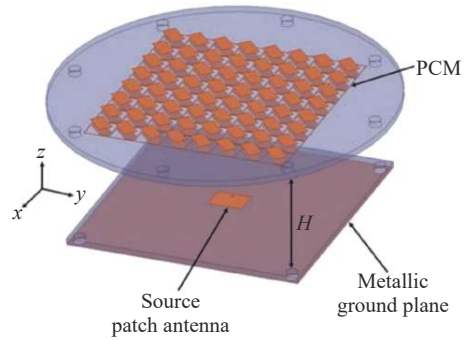

(a) Schematic diagram of the proposed antenna

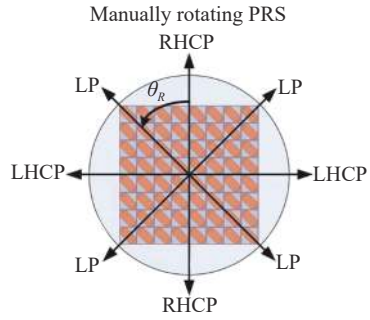

(b) Antenna polarization with different rotation angels θ_R

Fig. 16 Polarization reconfigurable FP antenna with manual rotating PRS [96]

3.6 Low RCS

Electronic warfare has become an important field considering the modern military background. The antenna is an important component of radar signal reception and transmission, which plays a key role in radar detection. Antennas, as scatterers, may be detected by radar. Therefore, the development of antenna stealth technology is of great value in the modern military field. The RCS is a physical quantity that reflects the stealth ability. Developing antennas with low RCS is an important research direction in the field of antennas, therefore, receiving significant attention from researchers. The realization methods of FP antennas with low RCS mainly include: (i) loading the AS; (ii) using a chessboard arranged metasurface (CAM); (iii) using a chessboard polarization conversion metasurface (CPCM); (iv) using a coding metasurface; (v) using a phase gradient metasurface (PGM).

Loading the AS is currently one of the important methods to realize low-RCS characteristics of FP antennas. Usually, this method is to employ resistance elements on the PRS, so that the RCS of the antenna is reduced due to the absorbing properties of the PRS. In 2014, Pan et al. implemented a low-RCS FP antenna by adopting a PRS with an AS [97]. The PRS was composed of a reflecting surface and an AS. The antenna gain enhancement was attributed to the FP cavity, and the RCS reduction was

owed to the AS. In 2016, Li et al. proposed an artificial composite material with broadband absorption and partial reflection characteristics to achieve a low-RCS FP antenna [98]. The artificial composite material was composed of an artificial composite material absorber and a PRS. The absorber was used to reduce the RCS of the antenna, while the PRS formed a cavity with ground to increase the gain. Later, Jiang et al. combined a reconfigurable metamaterial ground plane and AS to achieve a wideband RCS-reduced FP antenna [99]. In 2017, as shown in Fig. 17, a high gain FP antenna with in-band and out-of-band RCS reduction by using a novel partially reflecting and absorbing surface was presented [100]. This design not only integrates the AS on the PRS, but also surrounds the source with metamaterial absorbers, thereby achieving a better in-band and out-of-band RCS reduction for this antenna.

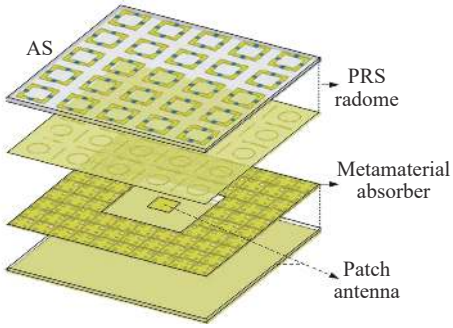

Fig. 17 Low-RCS FP antenna with AS [100]

Although the AS can effectively reduce the RCS of FP antennas, the resistive elements not only absorb the external incident wave but also the antenna's radiation energy, which limits the gain enhancement of the antenna. Recently, in order to improve the gain enhancement of FP antennas, CAMs have been used to achieve low RCS of FP antennas. In 2018, Hakim et al. implemented a low-profile, low-RCS FP antenna using a checkerboard AMC [101]. This design uses an AMC with the zero-degree reflection phase as the PRS of the FP antenna to obtain the low-profile characteristic, and adopts a checkerboard metasurface formed by two units with different reflection phases to reduce the RCS. In 2018, Zheng et al. used a CAM to achieve a wideband FP antenna with gain enhancement and RCS reduction characteristics [102]. Based on the principle of phase cancellation, this design uses two FSS units with a reflection phase difference of 180°±30° to form a CAM to reduce the RCS of the FP antenna. In 2019, Zarbakhsh et al. combined the phase cancellation principle, an FP resonant cavity and a sequential feeding technique to achieve a low-RCS, high-gain, broadband CP FP antenna [103]. The sequential feeding technique was used on the source antenna to obtain broadband circular polarization characteristics, and a CAM composed of two FSSs was employed as the PRS to obtain the broadband gain enhancement and RCS reduction characteristics of the antenna. In 2020, Liu et al. incorporated a hybrid partially reflecting surface into the CAM to design an FP antenna with wideband gain enhancement and RCS reduction [104]. The structure of this antenna is shown in Fig. 18. This design improves the 3 dB gain bandwidth and gain enhancement of the FP antenna, and achieves in-band RCS reduction.

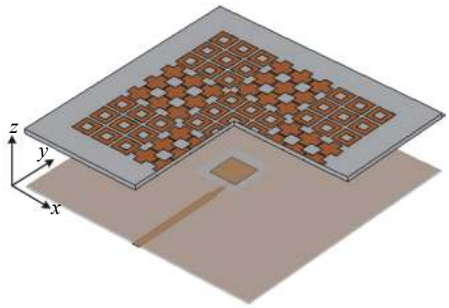

Fig. 18 Low-RCS FP antenna with CAM [104]

Adopting a CPCM is one of the important ways to realize the RCS reduction of an FP antenna. Generally, CPCMs are composed of a polarization conversion unit and its mirror unit etched on the substrate in a checkerboard arrangement. As the incident wave irradiates a CPCM, the reflection phases of the two symmetrical polarization conversion units have a perfect phase difference of 180°, so as to realize the interference cancellation of the reflected waves. In 2017, Li et al. implemented a wideband high-gain, low-RCS CP FP antenna based on a CPCM [105]. The CPCM consists of four sub-polarization conversion metasurfaces arranged in mirror images. The LP wave radiated by a slot antenna is converted into a CP wave after passing through the CPCM. This design expands the circular polarization bandwidth and reduces the RCS of the antenna. Later, Long et al. also designed a CPCM composed of PCM and PRS to realize a wideband low-RCS FP antenna [106]. In 2018, Zheng et al. proposed a low-RCS wideband CP FP antenna based on a polarization conversion metasurface array and a 2×2 slot antenna array [107]. In 2020, Liu et al. incorporated a small CPCM into a CPCM to construct an embedded CPCM for the design of a low-RCS FP antenna [108]. It demonstrates that a PCM can achieve wideband RCS reduction for FP antennas, while embedding a suitable small CPCM in a larger CPCM can reduce the in-band RCS of the antenna more effectively.

In addition, there are few investigations on the RCS reduction of FP antennas by using a coded metasurface and

PGM. Coding a metasurface can redirect the reflected wave, which requires the design of multiple PRS units for encoding. After encoding these units, an optimization algorithm will be employed to optimize the arrangement of the units, so as to obtain an optimized coding sequence on the PRS for RCS reduction. In 2017, Zhang et al. used the concept of coding a metasurface to realize an FP antenna with RCS reduction by the particle swarm optimization algorithm [109]. The PGM is composed of PRS units whose reflection phase gradient changes along a specified direction. It can reflect the incident wave to a desired direction, thus reducing the monostatic RCS of the antenna. In 2019, Jia et al. proposed two FP antennas with wideband RCS reductions by using two different PGMs. One PGM without a lossy layer is used to achieve an FP antenna with in-band RCS reduction and a high aperture efficiency. Meanwhile, a second PGM structure with the metamaterial absorber broadens the RCS reduction bandwidth of the FP antenna [110].

In summary, the stealth technology applied to antennas is of great significance in specific backgrounds. The methods to realize low-RCS FP antennas are mainly based on the principle of absorption, phase cancellation, and redirection of reflected waves. Note that it is a contradiction in principle to reduce the RCS of the antenna while achieving a high antenna gain. Therefore, the study of FP antennas with a high gain and wideband RCS reduction is one of the important research directions in this field.

4. Prospects

Since the characteristics of FP antennas include high gain and planar configuration, they have broad application prospects in wireless communications. Table 1 shows the performance comparison of some reported FP antennas. GBP is the gain-bandwidth product, and λ denotes the wavelength at the center frequency of the effective bandwidth in free space. Although many achievements have been made in the design of FP antennas, related research is still under development. Thus there are still some issues for FP antennas that can be studied in the future.

(i) Wideband printed PRS FP antennas. The PRS design of FP antennas can be divided into printed PRS and non-printed dielectric PRS. Most of the FP antennas with printed PRS can achieve high gains, but the GBPs seem to be limited. Moreover, it is difficult to simultaneously expand the 10 dB impedance bandwidth and the 3 dB gain bandwidth of FP antennas due to the increase in design complexity when using multilayer printed PRSs. Non-printed dielectric PRSs show excellent performance in terms of bandwidth extension and gain enhancement, but they may cause higher profiles. Therefore, it is important to study how to make the FP antenna with printed PRS obtain a wider operating bandwidth and a larger GBP, while having less impact on the profile height.

(ii) Multi-band FP antennas. According to the FP resonance condition, multi-band FP antennas need to excite the FP resonance at different operating frequencies under a fixed cavity height. This indicates that the wavelengths of multiple operating frequencies have a specific relationship, so that multiple operating frequencies cannot be arbitrarily selected. Moreover, the PRS has different reflection phase values at different frequencies, which increases the design complexity of the multi-band FP antenna. Therefore, realizing multi-band operating capabilities is a challenge, and it requires more advanced technologies to support the design of multi-band FP antennas.

(iii) Wideband low-profile FP antennas. Generally, the cavity height of an FP antenna is one-half of the operating wavelength. With the in-depth research on low-profile FP antennas, the narrowband low-profile high-gain FP antenna has produced many designs, and the cavity height can even be reduced to several tenths of the operating wavelength. However, there are few studies on low-profile FP antennas with wideband characteristics. The reason is that the coupling between source antenna and PRS is strengthened due to the decrease of the profile height. It is a great challenge to eliminate this coupling interference between them in a wide band. Therefore, how to realize FP antennas with wideband, low-profile, high-gain characteristics will be one of the important directions in the future.

(iv) Wideband CP FP antennas. CP antennas have great application value in wireless communications. Although the wideband CP FP antenna has made some achievements, its performance still needs to be further improved. The difficulty is how to expand the operating bandwidth of CP FP antennas and design a PRS that can be applied to achieve CP radiation over a wide band.

(v) Reconfigurable FP antennas. With the development of highly integrated, intelligent, and multi-functional wireless communication systems, reconfigurable antennas can better meet the needs of multi-channel communications. Reconfigurable antennas have important research value and broad application prospects. Many reconfigurable antennas employ varactor diodes, PIN diodes and MEMS. For these controllable elements, bias circuits are required, which will affect the radiation features of antennas and introduce limitations in their reconfigurable characteristics. Therefore, how to realize the reconfigurable FP antenna more conveniently and effectively is an important development trend.

Table 1 Comparison of the existing works

Reference	Feature	10 dB impedance bandwidth	Relative 3 dB gain bandwidth/%	Max. Gain (dBi/dBic)	GBP	Height	PRS technology
[11]	Low-profile	3.7 GHz	–	14.81	–	0.05λ	One-layer PRS
[15]	Low-profile	9.35 GHz	–	13.5	–	0.10λ	Substrate-integrated
[39]	Low-profile	10.5 GHz	–	15.0	–	0.30λ	Substrate-integrated
[40]	Low-profile	9.95 GHz	–	12.5	–	0.11λ	Substrate-integrated+AMC
[42]	Low-profile	9.8 GHz	–	13.5	–	0.12λ	PRS-AMC
[8]	Wideband	Around 5%	15.1	19.5	1346	1.41λ	Three-layer FSS
[9]	Wideband	8.6–11.2 (26.2%)	28	13.8	672	0.51λ	One-layer FSS
[16]	Wideband	Around 7.1%	6	17.44	333	0.95λ	Two-layer FSS
[49]	Wideband	Around 25%	15.7	16.2	654	0.54λ	One-layer FSS
[13]	Wideband	–	54.2	16.4	2366	1.01λ	TPG all-dielectric
[54]	Wideband	10–18.4 (59.2%)	57	20.2	5969	0.9λ	TPG all-dielectric
[56]	Wideband	5.8–16 (93.6%)	86.3	14.2	2270	1.31λ	Truncated three-layer dielectric
[59]	Dual-band	2.42–2.6 (7.2%) 5.2–5.8 (10.9%)	7 11	14.9 14.2	216 289	0.45λ 1.0λ	Two-layer FSS
[60]	Tri-band	5.1–5.5 (7.5%) 9.6–10.2 (6.1%) 14.4–16.0 (10.5%)	– – –	13.4 18.9 20	– – –	0.36λ 0.68λ 1.04λ	Two-layer FSS
[74]	Circular polarization	6.8–11.2 (48.9%)	50.3	14	1263	0.53λ	One-layer FSS
[80]	Frequency reconfigurable	4.55–4.7 (3.3%) 5.37–5.63 (4.7%)	11.9 8.2	13.1 17.1	243 421	0.42λ 0.50λ	One-layer reconfigurable PRS
[85]	Radiation pattern reconfigurable	5.5 GHz	–	10.4	–	0.46λ	One-layer FSS with PIN diodes
[20]	Wideband+polarization reconfigurable	2.2–2.72 (21%)	14.6	15.1	472	0.5λ	One-layer FSS
[96]	Polarization reconfigurable	10.3–11.22 (8.6%)	7.1	12.5	126	0.53λ	PCM
[78]	Circular polarization+ Low-RCS	10.5–10.78 (2.6%)	–	10.2	–	0.43λ	One-layer PRS +AS
[104]	Wideband+Low-RCS	8.64–12.07 (33.1%)	25.4	17.08	1297	0.68λ	One-layer FSS
[108]	Wideband + Low-RCS	8.48–12.21 (36.1%)	25.5	17.2	1338	0.73λ	One-layer embedded CPCM

5. Conclusions

FP antennas have characteristics of simple configurations, planar structure, high gain, low profile, and easy integration. They have broad application prospects in wireless communications. This paper reviews the analysis theories commonly used in FP antennas, with emphasis on leaky wave analysis and ray tracing. Moreover, it focuses on the design techniques of various capabilities of FP antennas, and evaluates the realization methods of each capability, including low-profile, wideband, multi-band, features as well as circular polarization, reconfigurability, and low RCS. Finally, this paper presents an outlook for further research directions, which provides significant guidance for future developments of FP.

References

[1] HOFSTETTER D, THORNTON R L. Measurement of optical cavity properties in semiconductor lasers by Fourier analysis of the emission spectrum. IEEE Journal of Quantum Electronics, 1998, 34(10): 1914–1923.

[2] WU B L, WANG M G, DONG Y, et al. Magnetic field sensor based on a dual-frequency optoelectronic oscillator using cascaded magnetostrictive alloy-fiber Bragg grating-Fabry Perot and fiber Bragg grating-Fabry Perot filters. Optics express, 2018, 26(21): 27628–27638.

[3] LI Y, ZHANG Y J, CHEN H W. Tunable self-injected Fabry-Perot laser diode coupled to an external high-Q Si3N4/SiO2 microring resonator. Journal of Lightwave Technology, 2018, 36(16): 3269–3274.

[4] BRAGINSKY V B, VYATCHANIN S P. Low quantum noise tranquilizer for Fabry-Perot interferometer. Physics Letters A, 2002, 293(5/6): 228–234.

[5] LI Z G, TIAN J J, JIAO Y Z, et al. Simultaneous measurement of air pressure and temperature using fiber-optic cascaded Fabry-Perot interferometer. IEEE Photonics Journal, 2018, 11(1): 1–10.

[6] VON TRENTINI G. Partially reflecting sheet arrays. IRE Trans. on Antennas and Propagation, 1956, 4(4): 666–671.

[7] MUHAMMAD S A, SAULEAU R, VALERIO G, et al.

Self-polarizing Fabry-Perot antennas based on polarization twisting element. IEEE Trans. on Antennas and Propagation, 2012, 61(3): 1032–1040.
[8] KONSTANTINIDIS K, FERESIDIS A P, HALL P S. Multilayer partially reflective surfaces for broadband Fabry-Perot cavity antennas. IEEE Trans. on Antennas and Propagation, 2014, 62(7): 3474–3481.
[9] WANG N Z, LIU Q, WU C Y, et al. Wideband Fabry-Perot resonator antenna with two complementary FSS layers. IEEE Trans. on Antennas and Propagation, 2014, 62(5): 2463–2471.
[10] ZEB B A, GE Y, ESSELLE K P, et al. A simple dual-band electromagnetic band gap resonator antenna based on inverted reflection phase gradient. IEEE Trans. on Antennas and Propagation, 2012, 60(10): 4522–4529.
[11] KELLY J R, KOKKINOS T, FERESIDIS A P. Analysis and design of sub-wavelength resonant cavity type 2-D leaky-wave antennas. IEEE Trans. on Antennas and Propagation, 2008, 56(9): 2817–2825.
[12] JI L Y, GUO Y J, QIN P Y, et al. A reconfigurable partially reflective surface (PRS) antenna for beam steering. IEEE Trans. on Antennas and Propagation, 2015, 63(6): 2387–2395.
[13] HASHMI R M, ESSELLE K P. A class of extremely wideband resonant cavity antennas with large directivity-bandwidth products. IEEE Trans. on Antennas and Propagation, 2015, 64(2): 830–835.
[14] GARDELLI R, ALBANI M, CAPOLINO F. Array thinning by using antennas in a Fabry-Perot cavity for gain enhancement. IEEE Trans. on Antennas and Propagation, 2006, 54(7): 1979–1990.
[15] LIU Z M, LIU S B, BIAN B R, et al. Metasurface-based low-profile high-gain substrate-integrated Fabry-Perot cavity antenna. International Journal of RF and Microwave Computer-Aided Engineering, 2019, 29(4): e21583.
[16] MATEOSEGURA C, FERESIDIS A P, GOUSSETIS G. Bandwidth enhancement of 2-D leaky-wave antennas with double-layer periodic surfaces. IEEE Trans. on Antennas and Propagation, 2014, 62(2): 586–593.
[17] LEE Y J, YEO J, KO K D, et al. A novel design technique for control of defect frequencies of an electromagnetic bandgap (EBG) superstrate for dual-band directivity enhancement. Microwave and Optical Technology Letters, 2004, 42(1): 25–31.
[18] QIN F, GAO S, WEI G, et al. Wideband circularly polarized Fabry-Perot antenna. IEEE Antennas and Propagation Magazine, 2015, 57(5): 127–135.
[19] LIU Z M, LIU S B, BORNEMANN J, et al. A wideband fabry-perot antenna with enhanced gain in the high frequency operating band by adopting a truncated field correcting structure. IEEE Trans. on Antennas and Propagation, 2021. DOI: 10.1109/TAP.2021.3090841.
[20] LIAN R N, TANG Z Y, YIN Y Z. Design of a broadband polarization reconfigurable Fabry-Perot resonator antenna. IEEE Antennas and Wireless Propagation Letters, 2018, 17(1): 122–125.
[21] GUZMAN-QUIROS R, WEILY A R, GOMEZ-TORNERO J L, et al. A Fabry-Perot antenna with two-dimensional electronic beam scanning. IEEE Trans. on Antennas and Propagation, 2016, 64(4): 1536–1541.
[22] XIE P, WANG G M, LI H P, et al. A dual-polarized two-dimensional beam steering Fabry-Perot cavity antenna with a reconfigurable partially reflecting surface. IEEE Antennas and Wireless Propagation Letters, 2017, 16: 2370–2374.
[23] HUANG C, PAN W B, MA X L, et al. A frequency reconfigurable directive antenna with wideband low-RCS property. IEEE Trans. on Antennas and Propagation, 2016, 64(3): 1173–1178.
[24] AKALIN T, DANGLOT J, VANBESIEN O, et al. A highly directive dipole antenna embedded in a Fabry-Perot type cavity. IEEE Microwave and Wireless Components Letters, 2002, 12(2): 48–50.
[25] GE Y H, SUN Z, CHEN Z G, et al. A high-gain wideband low-profile Fabry-Perot resonator antenna with a conical short horn. IEEE Antennas and Wireless Propagation Letters, 2016, 15: 1889–1892.
[26] MENG F, SHARMA S K. A wideband resonant cavity antenna with compact partially reflective surface. IEEE Trans. on Antennas and Propagation, 2019, 68(2): 1155–1160.
[27] OLINER A A, JACKSON D R, VOLAKIS J L. Antenna engineering handbook. New York: McGrawHill, 2007.
[28] SENGUPTA S, JACKSON D R, LONG S A. Modal analysis and propagation characteristics of leaky waves on a 2-D periodic leaky-wave antenna. IEEE Trans. on Microwave Theory and Techniques, 2018, 66(3): 1181–1191.
[29] ALMUTAWA A T, HOSSEINI A, JACKSON D R, et al. Leaky-wave analysis of wideband planar Fabry-Perot cavity antennas formed by a thick PRS. IEEE Trans. on Antennas and Propagation, 2019, 67(8): 5163–5175.
[30] ZHOU L, DUAN X, LUO Z J, et al. High directivity Fabry-Perot antenna with a nonuniform partially reflective surface and a phase correcting structure. IEEE Trans. on Antennas and Propagation, 2020, 68(11): 7601–7606.
[31] JACKSON D, ALEXOPOULOS N. Gain enhancement methods for printed circuit antennas. IEEE Trans. on Antennas and Propagation, 1985, 33(9): 976987.
[32] YANG H Y, ALEXOPOULOS N G. Gain enhancement methods for printed circuit antennas through multiple superstrates. IEEE Trans. on Antennas and Propagation, 1987, 35(7): 860–863.
[33] ZHAO T, JACKSON D R, WILLIAMS J T, et al. General formulas for 2-D leaky-wave antennas. IEEE Trans. on Antennas and Propagation, 2005, 53(11): 3525–3533.
[34] BOUTAYEB H, DENIDNI T A. Internally excited Fabry-Perot type cavity: power normalization and directivity evaluation. IEEE Antennas and Wireless Propagation Letters, 2006, 5: 159–162.
[35] GOUDARZI A, HONARI M M, MIRZAVAND R. Resonant cavity antennas for 5G communication systems: a review. Electronics, 2020, 9(7): 1080.
[36] ZHOU L, LI H Q, QIN Y Q, et al. Directive emissions from subwavelength metamaterial-based cavities. Proc. of the IEEE International Workshop on Antenna Technology: Small Antennas and Novel Metamaterials, 2005. DOI: 10.1109/IWAT.2005.1461045.
[37] WANG S, FERESIDIS A P, GOUSSETIS G, et al. High-gain subwavelength resonant cavity antenna based on metamaterial ground planes. IEE Proceedings—Microwaves, Antennas and Propagation, 2006, 153(1): 1–6.
[38] COSTA F, MONORCHIO A, MANARA G. Low-profile tunable and steerable Fabry-Perot antenna for software defined radio application. Proc. of the IEEE Antennas and Propagation Society International Symposium, 2010: 1–4.
[39] ZHU B, CHEN Z N, FENG Y J. Fully substrate-integrated high-gain thin Fabry-Perot cavity antennas. Proc. of the Asia-Pacific Microwave Conference, 2011: 602–605.
[40] SUN Y, CHEN Z N, ZHANG Y, et al. Subwavelength substrate-integrated Fabry-Perot cavity antennas using artificial magnetic conductor. IEEE Trans. on Antennas and Propagation, 2012, 60(1): 30–35.
[41] JI L, WANG J D, CHEN W D, et al. Substrate-integrated

Fabry-Perot cavity antenna fed by slot-coupled patch array for directivity enhancement. Proc. of the Asia-Pacific Microwave Conference, 2013: 1067–1069.
[42] LIU W, CHEN Z N, SEE T S P, et al. SIW-slot-fed thin beam-squint-free Fabry-Perot cavity antenna with low back-lobe levels. IEEE Antennas and Wireless Propagation Letters, 2014, 13: 552–554.
[43] NGUYEN T K, PARK I. Design of a substrate-integrated Fabry-Perot cavity antenna for K-band applications. International Journal of Antennas and Propagation, 2015, 2015: 373801.
[44] GAO Z D, SU M, TANG B H, et al. Low-profile circularly polarized Fabry-Perot resonator antenna array with substrate integrated waveguide feed network. Proc. of the IEEE International Symposium on Electromagnetic Compatibility, 2017: 1–4.
[45] GE Z C, ZHANG W X, LIU Z G, et al. Broadband and high-gain printed antennas constructed from Fabry-Perot resonator structure using EBG or FSS cover. Microwave and Optical Technology Letters, 2006, 48(7): 1272–1274.
[46] FERESIDIS A P, VARDAXOGLOU J C. A broadband high-gain resonant cavity antenna with single feed. Proc. of the First European Conference on Antennas and Propagation, 2006: 1–5.
[47] LIU Z G, ZHAN W X, FU D L, et al. Broadband Fabry-Perot resonator printed antennas using FSS superstrate with dissimilar size. Microwave and Optical Technology Letters, 2008, 50(6): 1623–1627.
[48] WU Z H, ZHANG W X. Broadband printed compound air-fed array antennas. IEEE Antennas and Wireless Propagation Letters, 2010, 9: 187–190.
[49] GE Y, ESSELLE K P, BIRD T S. The use of simple thin partially reflective surfaces with positive reflection phase gradients to design wideband, low-profile EBG resonator antennas. IEEE Trans. on Antennas and Propagation, 2012, 60(2): 743–750.
[50] PIRHADI A, BAHRAMI H, NASRI J. Wideband high directive aperture coupled microstrip antenna design by using a FSS superstrate layer. IEEE Trans. on Antennas and Propagation, 2012, 60(4): 2101–2106.
[51] LEGER L, MONEDIERE T, JECKO B. Enhancement of gain and radiation bandwidth for a planar 1-D EBG antenna. IEEE Microwave and Wireless Components Letters, 2005, 15(9): 573–575.
[52] HASHMI R M, ZEB B A, ESSELLE K P. Wideband high-gain EBG resonator antennas with small footprints and all-dielectric superstructures. IEEE Trans. on Antennas and Propagation, 2014, 62(6): 2970–2977.
[53] WU K L, YIN W Y, ZHANG L, et al. A wideband EBG resonator antenna with an extremely small footprint area. Microwave and Optical Technology Letters, 2015, 57(7): 1531–1535.
[54] BABA A A, HASHMI R M, ESSELLE K P. Achieving a large gain-bandwidth product from a compact antenna. IEEE Trans. on Antennas and Propagation, 2017, 65(7): 3437–3446.
[55] BABA A A, HASHMI R M, ESSELLE K P, et al. Compact high-gain antenna with simple all-dielectric partially reflecting surface. IEEE Trans. on Antennas and Propagation, 2018, 66(8): 4343–4348.
[56] NGUYEN-TRONG N, TRAN H H, NGUYEN T K, et al. Wideband Fabry-Perot antennas employing multilayer of closely spaced thin dielectric slabs. IEEE Antennas and Wireless Propagation Letters, 2018, 17(7): 1354–1358.
[57] LEE D H, LEE Y J, YEO J, et al. Design of novel thin frequency selective surface superstrates for dual-band directivity enhancement. IET Microwaves, Antennas and Propagation, 2007, 1(1): 248–254.
[58] ZEB B A, GE Y, ESSELLE K P. A single-layer thin partially reflecting surface for tri-band directivity enhancement. Proc. of the Asia-Pacific Microwave Conference, 2012: 559–561.
[59] ABDELGHANI M L, ATTIA H, DENIDNI T A. Dual- and wideband Fabry-Perot resonator antenna for WLAN applications. IEEE Antennas and Wireless Propagation Letters, 2017, 16: 473–476.
[60] QIN F, GAO S, LUO Q, et al. A triband low-profile high-gain planar antenna using Fabry-Perot cavity. IEEE Trans. on Antennas and Propagation, 2017, 65(5): 2683–2688.
[61] CHEN J Q, ZHAO Y J, GE Y, et al. Dual-band high-gain Fabry-Perot cavity antenna with a shared-aperture FSS layer. IET Microwaves, Antennas and Propagation, 2018, 12(13): 2007–2011.
[62] QIN F, GAO S S, LUO Q, et al, et al. A simple low-cost shared-aperture dual-band dual-polarized high-gain antenna for synthetic aperture radars. IEEE Trans. on Antennas and Propagation, 2016, 64(7): 2914–2922.
[63] XIE P, WANG G M, KONG X X, et al. Design of a novel metasurface for dual-band Fabry-Perot cavity antenna. International Journal of RF and Microwave Computer-Aided Engineering, 2017, 28(2): 1–7.
[64] CHEN C, LIU Z G, WANG H, et al. Metamaterial-inspired self-polarizing dual-band dual-orthogonal circularly polarized Fabry-Perot resonator antennas. IEEE Trans. on Antennas and Propagation, 2018, 67(2): 1329–1334.
[65] DENG C J, LI Y, ZHANG Z J, et al. A circularly polarized pattern diversity antenna for hemispherical coverage. IEEE Trans. on Antennas and Propagation, 2014, 62(10): 5365–5369.
[66] WANG A K, YANG L, ZHANG Y, et al. A novel planar dual circularly polarized endfire antenna. IEEE Access, 2019, 7: 64297–64302.
[67] TRAN H H, TA S X, PARK I. Single-feed, wideband, circularly polarized, crossed bowtie dipole antenna for global navigation satellite systems. Journal of Electromagnetic Engineering and Science, 2014, 14(3): 299–305.
[68] CHOI E C, LEE J W, LEE T K, et al. Circularly polarized S-band satellite antenna with parasitic elements and its arrays. IEEE Antennas and Wireless Propagation Letters, 2014, 13: 1689–1692.
[69] SHI J, WU X, QING X M, et al. An omnidirectional circularly polarized antenna array. IEEE Trans. on Antennas and Propagation, 2015, 64(2): 574–581.
[70] WEILY A R, ESSELLE K P, BIRD T S, et al. High gain circularly polarised 1-D EBG resonator antenna. IET Electronics Letters, 2006, 42(18): 1012–1013.
[71] LIU Z G, LU W B. Broadband design of circularly polarized high-gain Fabry-Perot resonator antenna with simple array thinning technique. Microwave and Optical Technology Letters, 2017, 59(12): 3171–3176.
[72] TRAN H H, LE T T, BUI C D, et al. Broadband circularly polarized Fabry-Perot antenna utilizing Archimedean spiral radiator and multi-layer partially reflecting surface. International Journal of RF and Microwave Computer-Aided Engineering, 2018, 29(3): 1–7.
[73] CAO W Q, LV X M, WANG Q Q, et al. Wideband circularly polarized Fabry-Perot resonator antenna in Ku-band. IEEE Antennas and Wireless Propagation Letters, 2019, 18(4): 586–590.
[74] TRAN H H, NGUYEN-TRONG N, NGUYEN T K. Low-profile wideband Fabry-Perot resonator antenna using artificial magnetic conductor surface. Microwave and Optical

Technology Letters, 2018, 61(2): 316–322.
[75] DIBLANC M, RODES E, ARNAUD E, et al. Circularly polarized metallic EBG antenna. IEEE Microwave and Wireless Components Letters, 2005, 15(10): 638–640.
[76] ORR R, GOUSSETIS G, FUSCO V. Design method for circularly polarized Fabry-Perot cavity antennas. IEEE Trans. on Antennas and Propagation, 2014, 62(1): 19–26.
[77] LIU Z G, LU W B. Low-profile design of broadband high gain circularly polarized Fabry-Perot resonator antenna and its array with linearly polarized feed. IEEE Access, 2017, 5(1): 7164–7172.
[78] REN J Y, JIANG W, ZHANG K Z, et al. A high-gain circularly polarized Fabry-Perot antenna with wideband low-RCS property. IEEE Antennas and Wireless Propagation Letters, 2018, 17(5): 853–856.
[79] WEILY A R, BIRD T S, GUO Y J. A reconfigurable high-gain partially reflecting surface antenna. IEEE Trans. on Antennas and Propagation, 2008, 56(11): 3382–3390.
[80] XIE P, WANG G M. Design of a frequency reconfigurable Fabry-Perot cavity antenna with single layer partially reflecting surface. Progress in Electromagnetics Research Letters, 2017, 70: 115–121.
[81] HAO Y, ALOMAINY A H, PARINI C G. Antenna-beam shaping from offset defects in UC-EBG cavities. Microwave and Optical Technology Letters, 2004, 43(2): 108–112.
[82] DEBOGOVIC T, PERRUISSEAU-CARRIER J. Array-fed partially reflective surface antenna with independent scanning and beamwidth dynamic control. IEEE Trans. on Antennas and Propagation, 2014, 62(1): 446–449.
[83] DEBOGOVIC T, PERRUISSEAU-CARRIER J, BARTOLIC J, et al. Partially reflective surface antenna with dynamic beamwidth control. IEEE Antennas and Wireless Propagation Letters, 2010, 9(3): 1157–1160.
[84] DEBOGOVIC T, PERRUISSEAU-CARRIER J. Dual-polarized beamwidth-reconfigurable Fabry-Perot antenna in monolithic MEMS technology. Proc. of the IEEE Antennas and Propagation Society International Symposium, 2013: 754–755.
[85] JI L Y, ZHANG Z Y, LIU N W. A two-dimensional beam-steering partially reflective surface (PRS) antenna using a reconfigurable FSS structure. IEEE Antennas and Wireless Propagation Letters, 2019, 18(6): 1076–1080.
[86] SULTAN F, MITU S S I. Superstrate-based beam scanning of a Fabry-Perot cavity antenna. IEEE Antennas and Wireless Propagation Letters, 2016, 15: 1187–1190.
[87] LAN J H, SUN B H, YAN W B, et al. A beam scanning Fabry-Perot cavity antenna for millimeter-wave applications. International Journal of RF and Microwave Computer-Aided Engineering, 2019, 29(5): 1–5.
[88] GUO C L, LIU F F, CHEN S, et al. Advances on exploiting polarization in wireless communications: channels, technologies, and applications. IEEE Communications Surveys & Tutorials, 2016, 19(1): 125–166.
[89] LV X L, WU B, ZHAO Y T, et al. Dual-band dual-polarization reconfigurable THz antenna based on graphene. Applied Physics Express, 2020, 13(7): 075007.
[90] JI L Y, QIN P Y, GUO Y J, et al. A wideband polarization reconfigurable antenna for WLAN applications. Proc. of the 10th European Conference on Antennas and Propagation, 2016: 1−3.
[91] HAN W W, OUYANG J, GUO Z, et al. A single-feed high-gain Fabry-Perot antenna with reconfigurable polarization capability. Proc. of the Cross Strait Quad-Regional Radio Science and Wireless Technology Conference, 2013: 279–281.
[92] VAIDYA A R, GUPTA R K, MISHRA S K, et al. Right-hand/left-hand circularly polarized high-gain antennas using partially reflective surfaces. IEEE Antennas and Wireless Propagation Letters, 2014, 13: 431–434.
[93] TRAN H H, PARK H C. A simple design of polarization reconfigurable Fabry-Perot resonator antenna. IEEE Access, 2020, 8: 91837–91842.
[94] LI W T, GAO S, CAI Y M, et al. Polarization-reconfigurable circularly polarized planar antenna using switchable polarizer. IEEE Trans. on Antennas and Propagation, 2017, 65(9): 4470–4477.
[95] NI C, LIU C Q, ZHANG Z X, et al. Design of broadband high gain polarization reconfigurable Fabry-Perot cavity antenna using metasurface. Frontiers in Physics, 2020, 8: 316.
[96] ZHANG X, CHEN C, JIANG S, et al. A high-gain polarization reconfigurable antenna using polarization conversion metasurface. Progress in Electromagnetics Research, 2020, 105: 1–10.
[97] PAN W B, HUANG C, CHEN P, et al. A low-RCS and high-gain partially reflecting surface antenna. IEEE Trans. on Antennas and Propagation, 2014, 62(2): 945–949.
[98] LI W Q, CAO X Y, GAO J, et al. Broadband RCS reduction and gain enhancement microstrip antenna using shared aperture artificial composite material based on quasi-fractal tree. IET Microwaves, Antennas and Propagation, 2016, 10(4): 370–377.
[99] JIANG H, XUE Z H, LI W M, et al. Low-RCS high-gain partially reflecting surface antenna with metamaterial ground plane. IEEE Trans. on Antennas and Propagation, 2016, 64(9): 4127–4132.
[100] MU J, WANG H, WANG H, et al. Low-RCS and gain enhancement design of a novel partially reflecting and absorbing surface antenna. IEEE Antennas and Wireless Propagation Letters, 2017, 16: 1903–1906.
[101] HAKIM L M V A, AANANDAN C K. Radar cross section reduction of low profile Fabry-Perot resonator antenna using checkerboard artificial magnetic conductor. Advanced Electromagnetics, 2018, 7(2): 76–82.
[102] ZHENG Y J, GAO J, ZHOU Y L, et al. Wideband gain enhancement and RCS reduction of Fabry-Perot resonator antenna with chessboard arranged metamaterial superstrate. IEEE Trans. on Antennas and Propagation, 2018, 66(2): 590–599.
[103] ZARBAKHSH S, AKBARI M, SAMADI F, et al. Broadband and high-gain circularly-polarized antenna with low RCS. IEEE Trans. on Antennas and Propagation, 2019, 67(1): 16–23.
[104] LIU Z M, LIU S B, ZHAO X, et al. Wideband gain enhancement and RCS reduction of Fabry-Perot antenna using hybrid reflection method. IEEE Trans. on Antennas and Propagation, 2020, 68(9): 6497–6505.
[105] LI K, LIU Y, JIA Y T, et al. A circularly polarized high-gain antenna with low RCS over a wideband using chessboard polarization conversion metasurfaces. IEEE Trans. on Antennas and Propagation, 2017, 65(8): 4288–4292.
[106] LONG M, JIANG W, GONG S X. Wideband RCS reduction using polarization conversion metasurface and partially reflecting surface. IEEE Antennas and Wireless Propagation Letters, 2017, 16: 2534–2537.
[107] ZHENG Q, GUO C J, DING J. Wideband and low RCS

planar circularly polarized array based on polarization conversion of metasurface. Microwave and Optical Technology Letters, 2018, 60(3): 784–789.
[108] LIU Z, LIU S, BORNEMANN J, et al. A low-RCS, high-GBP Fabry-Perot antenna with embedded chessboard polarization conversion metasurface. IEEE Access, 2020, 8: 80183–80194.
[109] ZHANG L, WAN X, LIU S, et al. Realization of low scattering for a high-gain Fabry-Perot antenna using coding metasurface. IEEE Trans. on Antennas and Propagation, 2017, 65(7): 3374–3383.
[110] JIA Y T, LIU Y, ZHANG W B, et al. High-gain Fabry-Perot antennas with wideband low monostatic RCS using phase gradient metasurface. IEEE Access, 2019, 7: 4816–4824.

Biographies

LIU Zhiming was born in 1989. He received his B.S. degree and M.S. degree from East China Institute of Technology, Fuzhou, China, in 2012 and Nanchang University, Nanchang, China, in 2015, respectively. He received his Ph.D. degree from the College of Electronic and Information Engineering, Nanjing University of Aeronautics and Astronautics, Nanjing, China, in 2019. He is a postdoctoral research fellow with the Department of Electrical and Computer Engineering, University of Victoria, Victoria, B.C., Canada. His current research interests include antennas, metamaterials and metasurface application.
E-mail: lzmedu@foxmail.com

BORNEMANN Jens was born in 1952. He received his M.S. and Ph.D. degrees, both in electrical engineering, from University of Bremen, Germany, in 1980 and 1984, respectively. From 1984 to 1985, he worked as an engineering consultant. In 1985, he joined University of Bremen, Germany, as an assistant professor. Since April 1988, he has been with the Department of Electrical and Computer Engineering, University of Victoria, Victoria, B.C., Canada, where he became a professor in 1992. From 1992 to 1995, he was a fellow of the British Columbia Advanced Systems Institute. In 1996, he was a visiting scientist at Spar Aerospace Limited (now MDA Space), Ste-Anne-de-Bellevue, Quebec, Canada, and a visiting professor at the Microwave Department, University of Ulm, Germany. From 1997 to 2002, he was a co-director of the Center for Advanced Materials and Related Technology, University of Victoria. In 2003, he was a visiting professor at the Laboratory for Electromagnetic Fields and Microwave Electronics, ETH Zurich, Switzerland. His research interests include radio frequency/wireless/microwave/millimeter-wave components and systems design, field-theory-based modeling of integrated circuits, feed networks and antennas.
E-mail: j.bornemann@ieee.org

LIU Shaobin was born in 1965. He received his Ph.D. degree in electronics science and technology from National University of Defense Technology in 2004. In 2003, he was already promoted as a professor. He is currently a professor of electromagnetic and microwave technology at Nanjing University of Aeronautics and Astronautics. His research interests include plasma stealthy antennas, microwave, radio frequency, and electromagnetic compatibility.
E-mail: lsb@nuaa.edu.cn

KONG Xiangkun was born in 1980. He received his Ph.D. degree in communication and information systems from Nanjing University of Aeronautics and Astronautics (NUAA) in 2015. He has been an associate professor in NUAA since his promotion in July 2015. He used to work at University of St. Andrews in the UK as an academic visitor supported by China Scholarship Council. His main research interests include electromagnetic properties of metamaterials, metamaterials and metasurface application, plasma photonic crystal, and computational electromagnetics.
E-mail: xkkong@nuaa.edu.cn